

ELASTIC MAXIMUM-ENERGY AND MAXIMUM-DIVERGENCE KIRCHHOFF MIGRATION

N. MARMALYEVSKYY*, Y. ROGANOV*, A. KOSTYUKEVYCH**, Z. GAZARIAN***, K. EPOV***

* *Ukrainian State Geological Prospecting Institute, 78 Avtozavodskaya St., 04114 Kiev, Ukraine*

** *Tesseral Technologies Inc., Suit 2905, 123 10th Avenue SW, Calgary, Alberta, Canada T2R 1K8*

*** *PetroAlliance, 40/3 Narodnogo Opolchenia St., Moscow, Russia*

Abstract

It is well known that for complex geological structures, prestack Kirchhoff depth migration employing first arrival (usually low energy) travel times produces inferior images when compared to an image obtained by using later events which contained more energetic travel times. This problem has been addressed by various authors, such as, Nichols (1996), Shin et al. (2003) and others. Although these methods calculate traveltimes and amplitudes of the most energetic arrivals, they all employ an approximation to a scalar one-way wave equation. In this presentation will illustrate the properties of elastic maximum energy Kirchhoff operators and their analogs computed with the use of vector wave equation in time wave field continuation.

Introduction

Nichols (1996) evaluated travel time arrivals of maximum-energy waves by phase advance of a small number of frequencies (8 to 16) via a frequency-domain wave field continuation. Shin et al. (2003), improved Nichols' algorithm by calculating maximum-energy times and amplitudes in intervals $[t, t+T]$, where t is time of first arrivals and T is user defined time window in which the operators are computed. This method utilizes a synthesized wave field obtained by summation of several complex frequencies. Complex frequencies are used in order to attenuate wraparound effects inherent in frequency domain wave equation solutions.

The use of the scalar wave equation in wave field depth extrapolation exhibits the following restrictions:

- thin-layering effects resulting an appearance of layer-induced anisotropy and seismic velocity dispersion;
- complex types of anisotropy that cannot be approximated by an analytically described weak-anisotropy model;
- refraction of waves, where an incident wave changes direction from downgoing to upgoing which can only be predicted by full wave field time continuation...

Moreover, computing Maximum Energy Operators (MEO) for Kirchhoff PSDM employing the full vector wave equation allows for the evaluation of additional wave modes used in migration. This class of waves may be defined as not just P-waves but as waves excited and received as P-waves. The use of new wave modes in migration may result in both improvement and deterioration of image quality.

In the later case, the operator is significantly affected by strong converted waves that are incident upon target boundaries but have no significant reflected energy. However, in such conditions, improved results can be obtained by using the maximum-divergence Kirchhoff operator (MDO).

Methodology of Computing the Operators

Following Nichols (1996) and Shin et al. (2003), we propose a new algorithm for determining travel time arrivals of maximum-energy events based on analyzing the vector components during a full vector wave field propagation in time. In such full wave field continuation both current values $(u_1; u_3)$ of particle velocity vector and stress components $\tau_{11}, \tau_{13}, \tau_{33}$ can be obtained. For computing the Kirchhoff MEO, the time of passage of the maximum energy $\frac{1}{2}\rho(u_1^2 + u_3^2)$ (where ρ is the density of the medium) through a spatial point $(x_1; x_3)$ is fixed under the condition that the wave is propagating predominantly downward, at this time step. The latter fact is determined by the sign of the quantity $\tau_{13}u_1 + \tau_{33}u_3$, which is proportional to the vertical (Z) component of Umov-Pointing vector.

In addition, computing the maximum of divergence operation $\frac{\partial u_1}{\partial x_1} + \frac{\partial u_3}{\partial x_3}$ the equivalent MDO's travel time arrival can be estimated under the same condition.

Data Examples

Properties of the above-described operators (MEO, MDO) are demonstrated on two model examples. Elastic synthetic seismograms were computed by solving the vector wave equation by finite-difference method.

The first model shown in Fig. 1 is provided by Petro Alliance (Moscow, Russia) and is a replica of a real section. It is characterized by abrupt velocity changes in the upper part of the section from 6000 m/s in carbonates to 2000 m/s in sand-shale indigenous deposits. Fig. 2 shows a seismic image obtained with the use of the elastic MEO. The image differs considerably from the model. Boundaries below 500 m are imaged above the model, and their shapes are distorted in the right part of the image. The reason for that is S-waves are interfering with the MEO. Fig. 3 shows time wave field snapshots formed assuming the maximum-energy criterion with excitation of a wave at the point of $X=5000\text{m}$ in the acoustic (a) and elastic (b) approximation.

It can be observed that the maximum-energy waves at the same spatial location differ quite considerably: (i.e. for $T=642$ ms in the case of acoustic approximation and $T=942$ ms in the case of elastic approximation). The reason for this difference is that in the second case the S-wave has the highest energy. Poor quality of the seismic image obtained with the use of MEO (Fig.2) is explained by the fact that despite the intense incident wave, converted reflected waves are of low intensity and they are not involved in computation of the operator.

Fig. 4 shows the seismic image obtained with the MDO. This image virtually completely coincides with the model. However, the image obtained with the use of the acoustic MEO (Fig. 5) is distorted against the model, especially in the right portion of the section. A poorer quality is evident in the image obtained with the acoustic MEO as compared to that of the elastic MDO. It shows to that there are some elements of the boundaries which are not illuminated exclusively by P-waves. In fact, they are illuminated by waves that have traveled along some part of the source-to-receiver path, as S-waves however are incident on the target boundary as P-waves.

The second model may be considered as a variation of the model given by Isaac and Lines (2002). In this case (Fig. 6), the overthrust formations are comprised of thin-periodic layers simulating an intercalation of carbonates and shales, overlying the target boundary with an anticlinal feature. In the upper part of the section, the horizontal element of this member is characterized by the following parameters: $\alpha_1=4000$ m/s, $\beta_1=2000$ m/s, $\rho_1=2350$ kg/m³, $\alpha_2=2000$ m/s, $\beta_2=1150$ m/s, $\rho_2=2010$ kg/m³, where α , β and ρ are P-wave, S-wave velocities and densities in carbonates and shales, respectively. Layer thickness in the member is 10 m with wave length of 60 m. A homogeneous quasi-anisotropic model may describe such a member. Vertical P-wave and S-wave velocities and Thomsen's parameters were calculated according to Backus (1962) averaging formulas and were as follows: $\alpha_{\perp}=2470$ m/s, $\beta_{\perp}=1450$ m/s, $\epsilon=0.32$, $\delta=0.03$. Within its sloping part, the thin-layer member is complicated enough introducing lateral velocity variations: for carbonates from 3500 m/s to 4000 m/s, and for shales from 1800 m/s to 2000 m/s.

Fig. 7 shows the seismic image obtained with the use of operator calculated on the principle of maximum vertical component of the wave field (MVCO). As is seen from the figure, the boundary under the overthrust (shown as a solid line on the images) was recovered practically in full conformity with the model.

Fig. 8 shows the image obtained with the use of the acoustic MEO. In this case, the image is less consistent with the model. This is true for both below-the-overthrust boundary and the bottom of the thin-layered member, whose intensity is reduced. The main reason for that is the neglect of layer-induced anisotropy and velocity dispersion in the computing of the operator, since in the acoustic approximation the medium behaves as homogeneous and isotropic in the low-frequency seismic range. Neglecting the conversion waves may also cause a significant impact. To demonstrate this, let us pay attention to the horizontal segment of the target boundary adjacent to the overthrust, which is marked with an arrow in Fig. 7. This section was obtained using the elastic MVCO. At the same time, in the case of operators which are not tuned to S-waves, i.e. acoustic MEO (Fig. 8), elastic MDO (Fig. 9) and elastic the one computed by first arrivals (Fig. 10), the above segment is not reconstructed. This verifies the fact that the MVCO shown in (Fig. 7) is constructed by waves that have arrived at these points as S-waves.

Tuning the elastic MEO (Fig. 11) in intensive converted waves results in obtaining a false focused boundary above the real one. In Fig. 11, such a boundary is marked with arrows. From analysis of this result, in particular, the following important conclusion can be drawn: the use of all kinds of waves for Kirchhoff migration (Operto et al, 2000) not allows yields the best result. It occurs when a wave exceeds the others in intensity. If the operator is not tuned in this wave, it may be considered a noise, and significant artifacts may appear on the resulting image. At the same time, the contribution of the operator to the true image will be insignificant due to a low-energy wave in which the operator was tuned.

Conclusions

Application of the vector wave equation in computing migration operators allows turning from a macro model of a medium to a micro model (thin-layer medium) that is much closer to the real one. A possibility also appears to use additional wave types in migration. As a result, more accurate seismic images may be obtained.

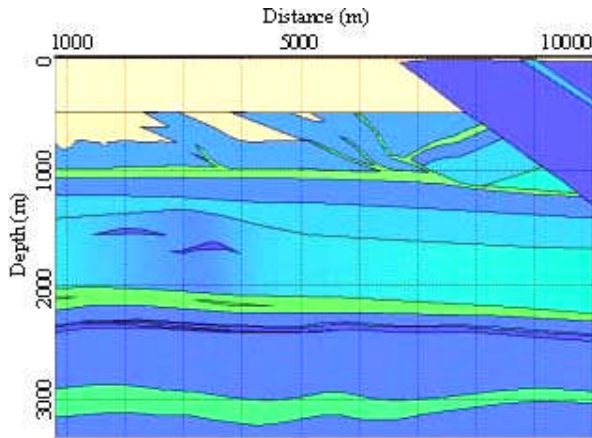


Fig.1. Model of carbonate overthrusts

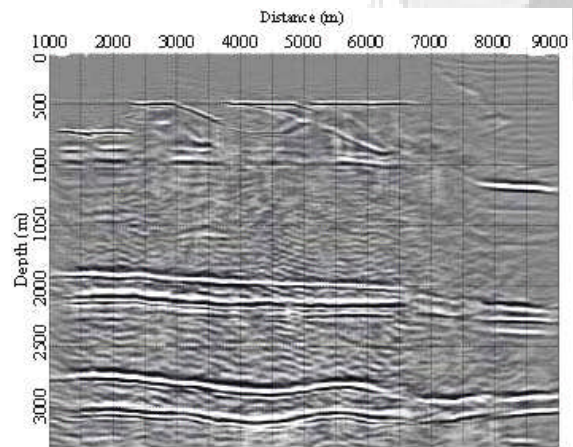


Fig.2. Pre-stack depth migration with maximum-energy elastic operator

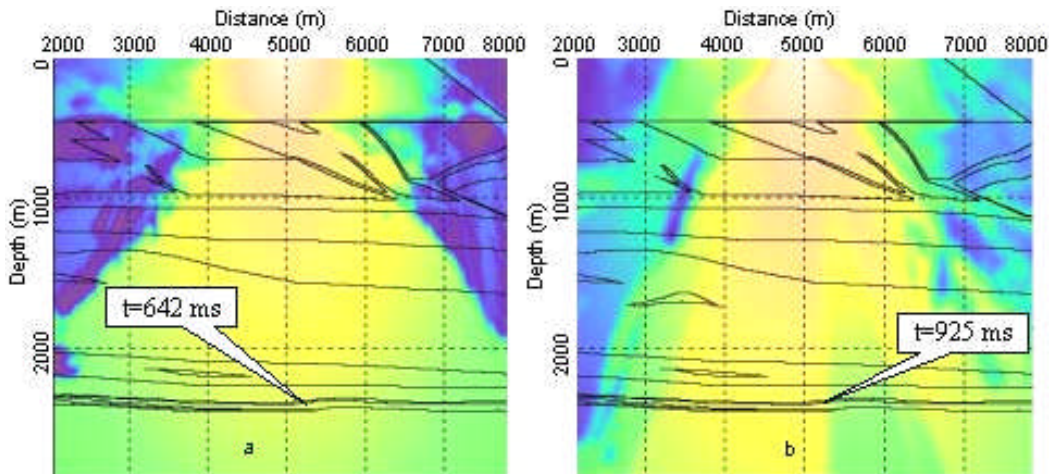


Fig.3. Propagation time of maximum-energy direct wave excited at the point of X=5000 m:
a - acoustic approximation; b - elastic approximation

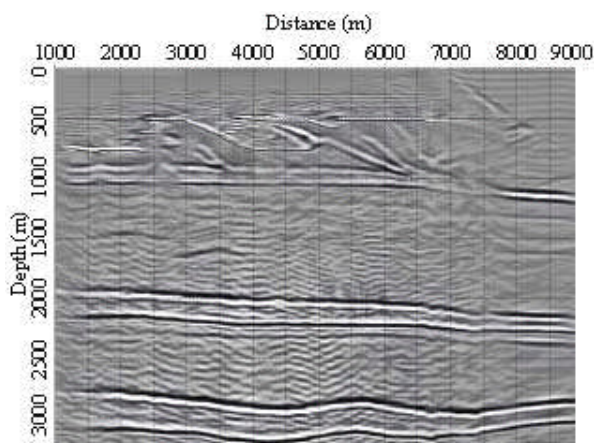


Fig.4. Pre-stack depth migration with maximum-divergence elastic operator

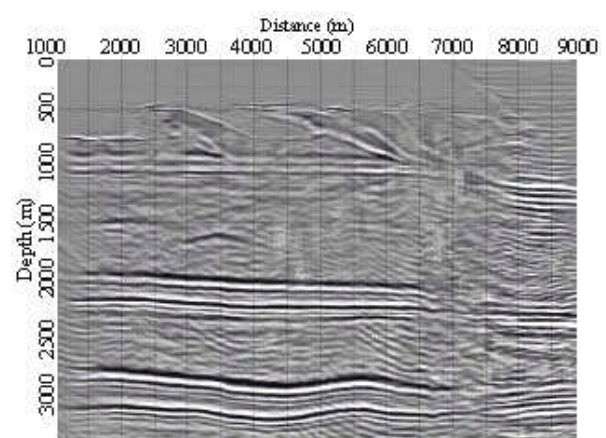
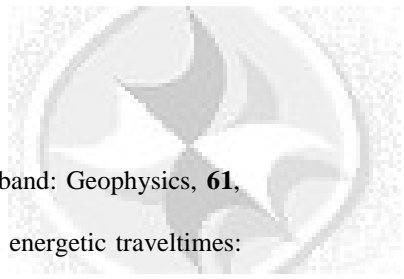


Fig.5. Pre-stack depth migration with maximum-energy acoustic operator

Acknowledgements

We would like to thank Dr. Constantine Tsingas of Kelman Technologies International and Dr. Ron Schmid (Calgary, Alberta) for their reviewing our paper and providing us with advice on the matter.



References

- Nichols, D. E., 1996, Maximum energy traveltimes calculated in the seismic frequency band: *Geophysics*, **61**, 253–263.
- Shin, C., Ko, S., Marfurt, K. J., and Yang, D., 2003, Wave equation calculation of most energetic traveltimes: *Geophysics*, **68**, 2040–2042.
- Backus, G., 1962, Long-wave elastic anisotropy produced by horizontal layering: *J. Geophys. Res.*, **67**, 4427–4440.
- Isaac, J. H. and Lines, L., 2002, Where's the reef?. *Recorder*, **27**, no. 3, 30-32.
- Operto, S., Xu, S., and Lambaré, G., 2000, Can we image quantitatively complex models with rays?: *Geophysics*, **65**, 1223–1238.

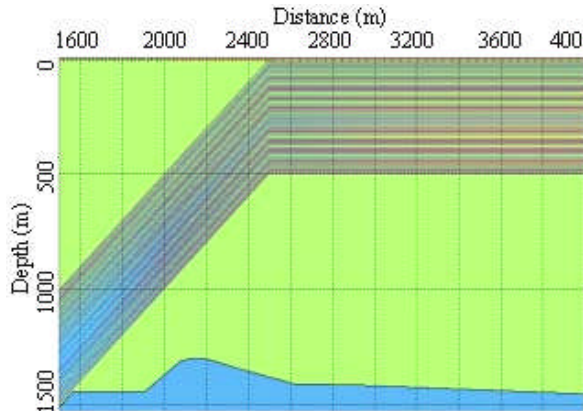


Fig. 6 Model of a thin-layered overthrust

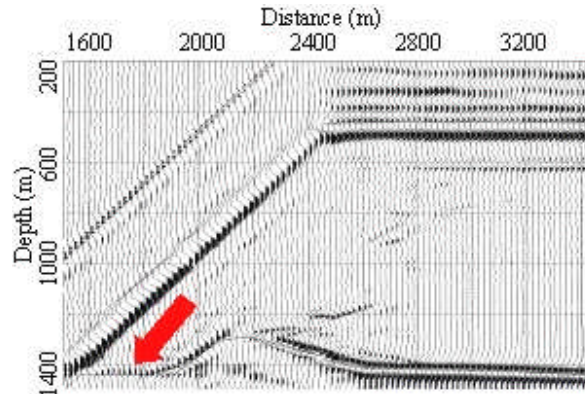


Fig.7 Seismic image obtained with the maximum-vertical-component operator

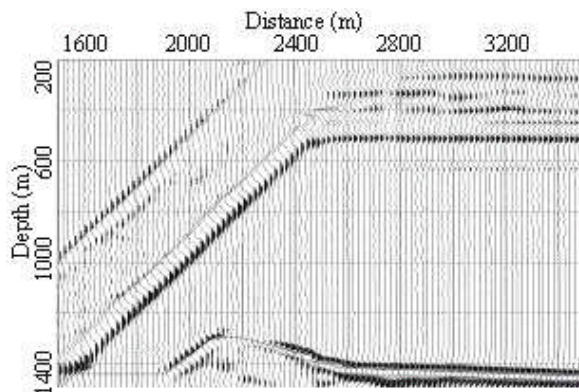


Fig.8 Seismic image obtained with the maximum-energy acoustic operator

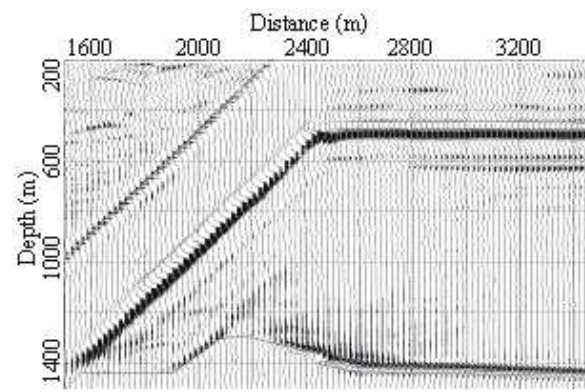


Fig.9 Seismic image obtained with the maximum-divergence elastic operator

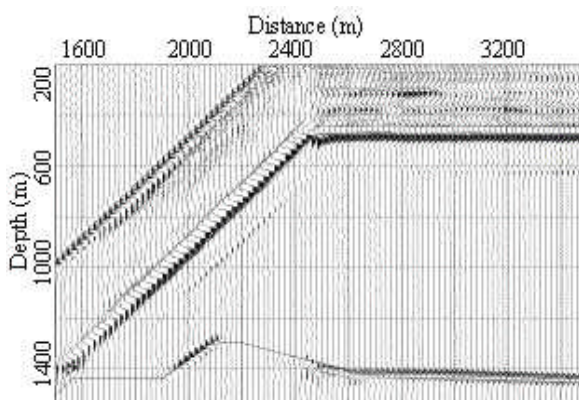


Fig.10 Seismic image obtained with operator computed on the basis of first arrival of elastic wave

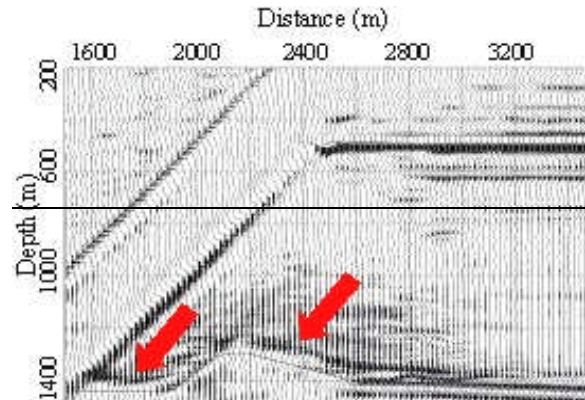


Fig.11 Seismic image obtained with the maximum-energy elastic operator